Flexural Design of Prestressed Concrete Beams Using FRP Tendons

Chad R. Burke, P.E.
Design Engineer
CH2M-Hill
Redding, California

Fiber Reinforced Polymer (FRP) tendons are being considered for design in structures exposed to aggressive environments or where non-metallic properties are desired. FRP tendons require considerable attention to detail during the design process. This paper presents a unified approach for the flexural design of beams with FRP tendons. Equations for flexural strength are presented, failure modes are defined, calibrations with test data are presented, and strength reduction factors are recommended. A test program validates the design approach and provides some serviceability data. Conclusions from the test program and design recommendations are provided.

Charles W. Dolan Ph.D., P.E.
Professor
Civil and Architectural Engineering
University of Wyoming
Laramie, Wyoming

Flexural testing of Fiber Reinforced Polymer (FRP), prestressed concrete beams began in Japan in the mid 1980s under a nationally coordinated program to develop design guidelines for concrete reinforced or prestressed with FRP tendons. Work began in Europe and in the United States in the late eighties.[1,2]

Several attempts have been made to develop design guidelines for FRP reinforcement, and these are in various states of completion. The lack of uniform testing procedures, material definitions, and reporting procedures has caused great difficulty in developing guidelines. Several of the developing design guidelines are evaluated and compared by Gilstrap.[3]

Methods for evaluating the flexural strength of an FRP prestressed beam originated in 1991[2] and were refined in 1996.[4,5] This paper presents a unified approach to flexural design of FRP prestressed members. Derivation of the flexural strength equations and calibration of these equations against test beams taken from the published literature is presented. An experimental confirmation of flexural behavior and other aspects of beam design allows an evaluation of serviceability performance of FRP prestressed beams. Design recommendations and strength reduction factors are recommended.

THEORETICAL DEVELOPMENT OF FLEXURAL CAPACITY

FRP tendons behave linearly elastically to failure. The industry trend is to define the tendon performance by the design strength of the tendon. The methods of defining the design strength and alternative approaches to defining tendon strength are discussed below. These definitions are essential to understanding the failure modes of an FRP prestressed structure and the corresponding strength reduction factors used in design.

The basis for the strength design methodology is the balanced ratio. The balanced ratio, ρ_b, is the reinforcement ratio at which simultaneous concrete compression and tendon rupture failure occurs. Any reinforcement ratio above this value leads to a primary concrete compression failure, while any reinforcement ratio below the balanced ratio indicates a tendon rupture failure. The stress and strain conditions for the balanced ratio are shown in Fig. 1.

The balanced ratio for FRP prestressed beams is similar to the balanced ratio used in reinforced concrete design to ensure ductile behavior. The behavior is different than that for steel tendons because FRP tendons are a brittle material. This leads to the FRP balanced ratio being an indicator of the failure mode rather than an assurance of ductility. By the traditional definition of ductility, beams reinforced or prestressed with FRP materials are not ductile.

At the same time, the strain to failure of an FRP tendon is greater than the strain for a steel tendon to reach a yield state. Consequently, beams prestressed with FRP tendons may exhibit large deformations prior to failure. The deformations are on the same order of magnitude as beams prestressed with steel tendons and the beams provide corresponding warning of incipient failure. In this paper, and for general use with a FRP prestressed beam, "under-reinforced" implies a tendon failure and "over-reinforced" implies a primary concrete compression failure.

Upon completion of the balanced ratio formulation, flexural design relationships for both over-reinforced and under-reinforced members are developed for bonded tendons. Because FRP tendons are linearly elastic to failure, draping or harping of tendons results in a loss of tendon strength in the vicinity of the harping or draping points. Strength reduction due to curvature of the tendons must be included in the design calculations based on the tendon radius of curvature at the deflection points.

Definition of Tendon Strength

A key design issue for FRP tendons is the definition of tendon strength. Due to the lack of a yield plateau or strain-hardening region, the designer must ensure that the design strength of the tendon is not exceeded in service.

Due to the variability in the tendon break strength, three different methods for reporting break strength have been used. First, the mean tensile strength is reported. Second, a 95 percent inclusion strength is reported. The 95 percent inclusion is 1.65 standard deviations less than the mean strength. Third, the "design strength" is reported. The design strength is the mean break strength reduced by three standard deviations.

Note that Japanese tendon manufacturers provide a "guaranteed break strength" for their tendons, which corresponds to the design strength. Often, neither the mean strength nor the standard deviation is reported in the literature. One consequence of this omission is that authors who report design strength tend to under-predict the capacity of a member.

Industry practice reports the gross cross-sectional area of a prefabricated tendon and the tendon stress is reported based on the gross area. FRP tendon sections consist of 50 to 70 percent fibers by volume and the remaining cross section is a polymer resin. Only the fibers contribute to the strength. Therefore, the ultimate stresses for FRP tendons based on the gross cross section are lower than the parent fiber strength reported in the literature.

Balanced ratio

The balanced ratio, ρ_b, is based on strain compatibility in the cross section and is calculated using four basic assumptions: the ultimate concrete compression strain is $\varepsilon_{cu} = 0.003$, the nonlinear behavior of the concrete is modeled using an equivalent rectangular stress block, tendon failure is defined as the ultimate tensile strain of the tendon, ε_{pu}, and the prestressing tendons are placed in a single layer. These conditions are illustrated in Fig. 1.

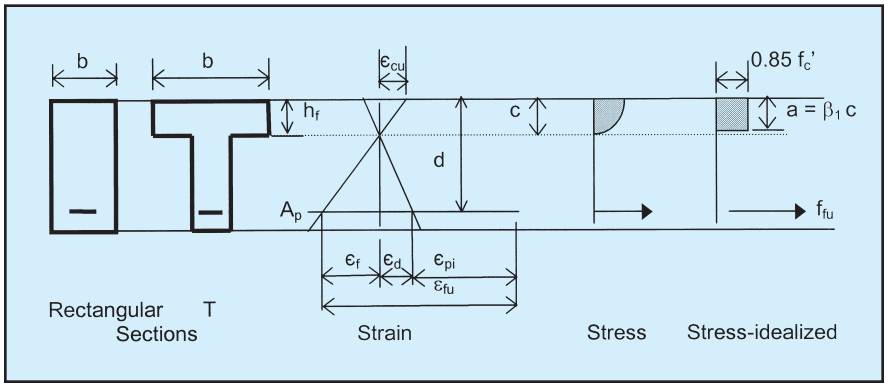

Fig. 1. Balanced ratio showing stress and strain conditions.

The balanced ratio is valid for both flanged and rectangular sections provided that the depth of the compression block is within the depth of the flange. The equation for the balanced ratio is given in Eq. (1):

$$\rho_b = 0.85\beta_1 \frac{f'_c}{f_{fu}} \frac{\varepsilon_{cu}}{\varepsilon_{cu} + \varepsilon_{fu} - \varepsilon_{pi}} \quad (1)$$

where

β_1 = factor defined as the ratio of the equivalent rectangular stress block depth to the distance from the extreme compression fiber to the neutral axis depth
f'_c = specified compressive strength of concrete
f_{fu} = ultimate tensile stress of tendon
ε_{cu} = concrete ultimate compression strain, 0.003
ε_{pi} = initial prestressing strain
ε_{fu} = ultimate strain capacity of tendon

Parameters β_1, f'_c, and ε_{cu} are material properties of the concrete, f_{fu} and ε_{fu} are tendon material properties, while the initial prestress, ε_{pi}, is chosen by the designer based upon the level of desired prestress and the type of tendons being used.

One conservative simplification is included in the formulation of the balanced ratio. The strain needed to decompress the tendon, ε_d, is ignored. This is a conservative assumption because ε_d is a negative value and it has an order of magnitude smaller than the other strains.

To evaluate Eq. (1), only the material properties and the initial prestress level must be known. The tendon supplier provides the ultimate tensile stress and strain for the tendon. If the tendon design strength is reported, the balanced ratio will slightly under-predict the transition from tendon failure to the concrete compressive failure mode.

Under-Reinforced Beams

Beams with a reinforcement ratio, ρ, less than ρ_b, fail by tendon rupture and are divided into two different conditions: very under-reinforced beams and under-reinforced beams. These two conditions are identified because a designer may be concerned that a single formulation for flexural strength may not properly represent the flexural behavior if the concrete is not strained into the nonlinear zone.

Very under-reinforced beams have reinforcement ratios less than half of ρ_b, and a nominally linear stress-strain behavior in the concrete up to the point of tendon failure. Such beams could be more precisely defined as having a concrete compressive stress at failure of less than $0.45 f'_c$.

Using $0.5\rho_b$ provides a computationally easier solution and avoids complex stress checks of the section. The nominal moment capacity, M_n, of the very under-reinforced beam is based on the tendon strength and the internal moment arm for an elastic section. The tendon strength is:

$$T_n = A_p f_{fu} = \rho b d f_{fu} \quad (2)$$

where

A_p = area of FRP tendon
f_{fu} = ultimate tensile strength of tendon
ρ = reinforcement ratio = A_p/bd
b = width of compression face
d = distance from centroid of outermost reinforcement to extreme compression fiber

Summing the moment of the forces around the compression centroid gives the nominal moment capacity:

$$M_n = \rho\, b\, d^2 f_{fu} (1 - k/3) \quad (3)$$

where

$$k = \sqrt{(\rho n)^2 + 2\rho n} - \rho n \quad (4)$$

and n is the modular ratio.

Under-reinforced beams have reinforcement ratios between $0.5\rho_b$ and ρ_b. These beams encounter significant nonlinear behavior in the concrete prior to tendon failure. Use of a rectangular stress block, the tensile capacity of the tendon given in Eq. (2), and summing moments about the centroid of the rectangular equivalent compression block results in:

$$M_n = \rho b d f_{fu} \left(d - \frac{a}{2} \right) \quad (5)$$

where

M_n = nominal moment capacity of section
a = depth of equivalent rectangular compression block determined by equilibrium of forces on cross section as shown in Eq. (6):

$$a = \frac{\rho b d f_{fu}}{0.85 f'_c} \quad (6)$$

Modification of this equation is required when multiple layers of reinforcement are used. The outermost tendon layer is more highly strained and will rupture first.

The remaining tendon layers may be unable to carry the load and a progressive failure of the beam will occur. As a result, the computation of the balanced ratio and the predicted moment capacity needs to be adjusted for variation in depth and stress level. These modifications are developed elsewhere.[6]

Over-Reinforced Beams

In over-reinforced beams, the moment capacity is found by equilibrium and compatibility similar to under-reinforced beams. In this case, the strain in the tendon is unknown and the concrete stress field is represented with an equivalent rectangular stress block. The neutral axis is located by solving a series of strain compatibility equations to locate the neutral axis.

The depth to the neutral axis is defined as $c = k_u d$, where c is the depth from the extreme compression fiber to the neutral axis. The coefficient k_u is defined by Eq. (7):

$$k_u = \sqrt{\rho\lambda + \left[\frac{\rho\lambda}{2} \left(1 - \frac{\varepsilon_{pi}}{\varepsilon_{cu}} \right) \right]^2} - \frac{\rho\lambda}{2} \left(1 - \frac{\varepsilon_{pi}}{\varepsilon_{fu}} \right) \quad (7)$$

where λ is a material constant defined in Eq. (8) using the tendon elastic modulus, E_f:

$$\lambda = \frac{E_f \varepsilon_{cu}}{0.85 f'_c \beta_1} \quad (8)$$

The above relationships result in the depth to the compression block being

Table 1. Calibration of flexural strength calculations.

Beam No.	Source No.	Tendon type	Condition	f'_c MPa	P_1 kN	A_p mm²	b mm	d mm	ρ	M_{exp} kN-m	M_n kN-m	$M_{exp}/\phi M_n$ Ratio ϕ=1.0	Ratio ϕ=0.9	Ratio ϕ=0.85	Ratio ϕ=0.80	Ratio ϕ=0.75	Ratio ϕ=0.70
Slab1	9	Aramid	Over-reinforced	69.2	33	88.8	280	70	0.00453	14.25	20.54	0.69	0.77	0.82	0.87	0.92	0.99
BA-1M	13	Aramid	Over-reinforced	57.7	684	900	230	405	0.00966	664.4	540.25	1.23	1.37	1.45	1.54	1.64	1.76
BA-6Y	13	Aramid	Over-reinforced	57.2	684	900	230	405	0.00966	654.6	537.18	1.22	1.35	1.43	1.52	1.62	1.74
Fibra1	14	Aramid	Over-reinforced	41.2	43.8	126	127	162	0.00612	38.9	34.45	1.13	1.25	1.33	1.41	1.51	1.61
Fibra2	14	Aramid	Over-reinforced	41.2	43.8	126	127	183	0.00542	46.1	42.35	1.09	1.21	1.28	1.36	1.45	1.55
Fibra3	14	Aramid	Over-reinforced	41.2	43.8	126	127	183	0.00542	52.9	42.35	1.25	1.39	1.47	1.56	1.67	1.78
AFRP-40	15	Aramid	Over-reinforced	35	80	196	150	235	0.00556	50	73.22	0.68	0.76	0.80	0.85	0.91	0.98
AFRP-80	15	Aramid	Under-reinforced	85	90	196	150	235	0.00556	50	56.80	0.88	0.98	1.04	1.10	1.17	1.26
CFCC1	14	Carbon	Over-reinforced	36.1	85.4	76	127	179	0.00334	47.2	38.10	1.24	1.38	1.46	1.55	1.65	1.77
CFCC2	14	Carbon	Over-reinforced	36.1	85.4	76	127	179	0.00334	47.2	38.10	1.24	1.38	1.46	1.55	1.65	1.77
CFCC3	14	Carbon	Over-reinforced	36.1	85.4	76	127	149	0.00402	33.3	28.04	1.19	1.32	1.40	1.48	1.58	1.70
R-4-5.H	16	Carbon	Over-reinforced	47	296.6	201	200	280	0.00359	155.9	189.83	0.82	0.91	0.97	1.03	1.09	1.17
R-4-5.V	16	Carbon	Over-reinforced	47	296.6	201	200	255	0.00394	157.4	162.29	0.97	1.08	1.14	1.21	1.29	1.39
R-4-7.V	16	Carbon	Over-reinforced	47	415.2	201	200	255	0.00394	170.8	170.21	1	1.12	1.18	1.25	1.34	1.43
3	4	Carbon	Under-reinforced	35.3	68	55.7	100	100	0.00557	10.29	8.07	1.28	1.42	1.50	1.59	1.70	1.82
4	4	Carbon	Under-reinforced	35.3	68	55.7	100	100	0.00557	10.5	8.07	1.3	1.45	1.53	1.63	1.74	1.86
5	4	Carbon	Under-reinforced	35.3	68	30.4	100	100	0.00304	7.29	5.16	1.41	1.57	1.66	1.77	1.88	2.02
CTL3	11	Carbon	Under-reinforced	47.9	187.1	152	254	210	0.00285	66.6	64.82	1.03	1.14	1.21	1.28	1.37	1.47
CTL6	11	Carbon	Under-reinforced	75.2	185.6	152	254	210	0.00285	68.1	66.78	1.02	1.13	1.20	1.27	1.36	1.46
CTL9	11	Carbon	Under-reinforced	53.3	188.8	152	254	210	0.00285	66.5	65.37	1.02	1.13	1.20	1.27	1.36	1.45
CFCC1	12	Carbon	Under-reinforced	59.78	84.52	76	254	76.2	0.00393	11.32	11.26	1.01	1.12	1.18	1.26	1.34	1.44
CFCC2	12	Carbon	Under-reinforced	58.61	84.52	76	254	76.2	0.00393	10.02	11.24	0.89	0.99	1.05	1.11	1.19	1.27
T-4-5.H	16	Carbon	Under-reinforced	47	296.6	201	600	280	0.0012	186.1	158.74	1.17	1.30	1.38	1.47	1.56	1.68
T-4-5.V	16	Carbon	Under-reinforced	47	296.6	201	600	255	0.00131	172.2	143.91	1.2	1.33	1.41	1.50	1.60	1.71
T-4-7.V	16	Carbon	Under-reinforced	47	415.2	201	600	255	0.00131	179.5	143.91	1.25	1.39	1.47	1.56	1.66	1.78
T-2-5.V	16	Carbon	Under-reinforced	47	148.3	101	600	255	0.00066	101.5	73.79	1.38	1.53	1.62	1.72	1.83	1.96
R-2-5.V	16	Carbon	Under-reinforced	47	148.3	101	200	255	0.00197	100.6	70.12	1.43	1.59	1.69	1.79	1.91	2.05
Leadline1	14	E-Glass	Over-reinforced	39	41.1	120	127	157	0.00601	31	31.33	0.99	1.10	1.16	1.24	1.32	1.41
Leadline2	14	E-Glass	Over-reinforced	39	41.1	120	127	191	0.00494	43	43.69	0.98	1.09	1.16	1.23	1.31	1.41
Leadline3	14	E-Glass	Over-reinforced	39	41.1	120	127	191	0.00494	40.2	43.69	0.92	1.02	1.08	1.15	1.23	1.31

Sources of beam data:

	Ref. No.
4. Kakizawa, 1993	10
9. Taerwe, 1995	11
11. Arockiasamy, 1995	12
12. Zhao, 1994	13
13. Niitani, 1997 (Draft)	14
14. Currier, 1995	15
15. Gowripalan, 1996	16
16. Abdelrahman, 1997	5

All Beams

Mean =	1.097	1.219	1.290	1.371	1.462	1.567
Standard deviation =	0.196	0.218	0.231	0.245	0.261	0.280

Normally Reinforced Beams

Mean =	1.161	1.290	1.366	1.452	1.548	1.659
Standard deviation =	0.188	0.209	0.221	0.235	0.251	0.269

Over-Reinforced Beams

Mean =	1.040	1.156	1.224	1.300	1.387	1.486
Standard deviation =	0.190	0.212	0.224	0.238	0.254	0.272

Aramid Tendon Beams

Mean =	1.021	1.135	1.202	1.277	1.362	1.459
Standard deviation =	0.237	0.263	0.278	0.296	0.316	0.338
For *Mean* - $B\sigma$ = 1.0, B =	0.091	0.513	0.725	0.936	1.147	1.358

Carbon Tendon Beams

Mean =	1.149	1.277	1.352	1.437	1.532	1.642
Standard deviation =	0.178	0.198	0.209	0.222	0.237	0.254
For *Mean* - $B\sigma$ = 1.0, B =	0.840	1.403	1.684	1.965	2.247	2.528

$a = \beta_1 c = \beta_1 k_u d$. Summing the moment of forces about the tendon leads to Eq. (9) for the nominal moment capacity for an over-reinforced beam:

$$M_n = 0.85 f'_c b \beta_1 k_u d^2 \left(1 - \frac{\beta_1 k_u}{2}\right) \quad (9)$$

Calibration of Design Equations Against Available Test Data

A review of published material identified 30 test specimens for calibration (see Table 1). Each beam in Table 1 was analyzed to determine the balanced ratio and probable failure mode. The nominal moment capacity was computed using the appropriate equation. Interpretation of test data from the literature is complicated because authors have not consistently reported tendon strength or prestress tendon area.

The use of mean break strength or the design strength makes a significant difference in the predictions. Each paper was reviewed in detail. In most cases, North American and European authors reported mean strength while Japanese authors reported design strength. In some instances, it is impossible to discern the tendon properties.

The ratio of the reported experimental moment capacity to theoretical moment capacity is presented for each of the test specimens. An analysis of the ratio of experimental to predicted strength was conducted. The mean value and the standard deviation in the ratio are computed for different failure modes, tendon types and strength reduction factors.

The strength reduction factor was varied from 1.0 to 0.7 in order to evaluate the number of specimens that are safely predicted with each reduction factor. Values are not calculated for beams with glass tendons, since glass is not recommended for use in pretensioned beams due to stress corrosion and creep-rupture limitations.[7]

For all cases, the mean value of the experimental strength to the predicted strength slightly exceeds 1.0. This implies that the predictive equations are suitable for design. The beam data are also analyzed by failure type and tendon type. Table 1 indicates that predictions of under-reinforced beams are slightly more conservative than for over-reinforced beams.

Carbon tendons provide more conservative predictions than aramid tendons. This latter conclusion is influenced by the fact that the CFCC beams are based on the tendon design strength rather than the mean strength. Since the correlation between mean and design strength is not provided, the higher apparent performance of the carbon tendons is not unexpected.

The use of strength reduction factors, ϕ, allows the ratio of experimental to nominal moment capacity to be adjusted so that the probability of failure is minimized. For a 95 percent inclusion of all data, the ratio of experimental to predicted strength should be raised to 1.0 plus 1.65 standard deviations.

Table 1 presents summaries based on the failure mode and on the tendon material. Because the section strength reduction factor is philosophically tied to material performance rather than failure mode, the selection and recommendation of the value for the strength reduction factor is based on the tendon type.

Based on data in Table 1, a strength reduction factor of 0.85 is recommended for carbon tendons and 0.70 for aramid tendons. Table 1 also shows that strength reduction factors of 1.0 and 0.9 under-predict too many samples.

Analytic Validation of Design Equations

An analytic calibration of the design equations consisted of a parametric study that examined the behavior of the equations over a large range of reinforcement ratios and compared the equation predictions to an alternative method of section analysis. The alternative analysis consisted of a computer program that simulates a section by dividing it into thin lamina with the material properties being defined individually for each lamina.

The program varies the compression strain at the top of the member over a user-defined range and uses an iterative process to solve for the neutral axis location and moment capacity at each compression strain level. The program uses a nonlinear stress-strain relationship for the concrete behavior defined by Collins and Mitchell,[8] and a linear stress-strain relationship for the tendons.

Two cross sections and four different tendon types were examined. A typical calibration curve is shown in Fig. 2. This study accomplished three objectives:

First, the analysis confirmed that the very under-reinforced and under-reinforced equations resulted in values that did not diverge until the over-reinforced range. Thus, while the two equations are useful for analysis, only Eq. (5) is needed for design.

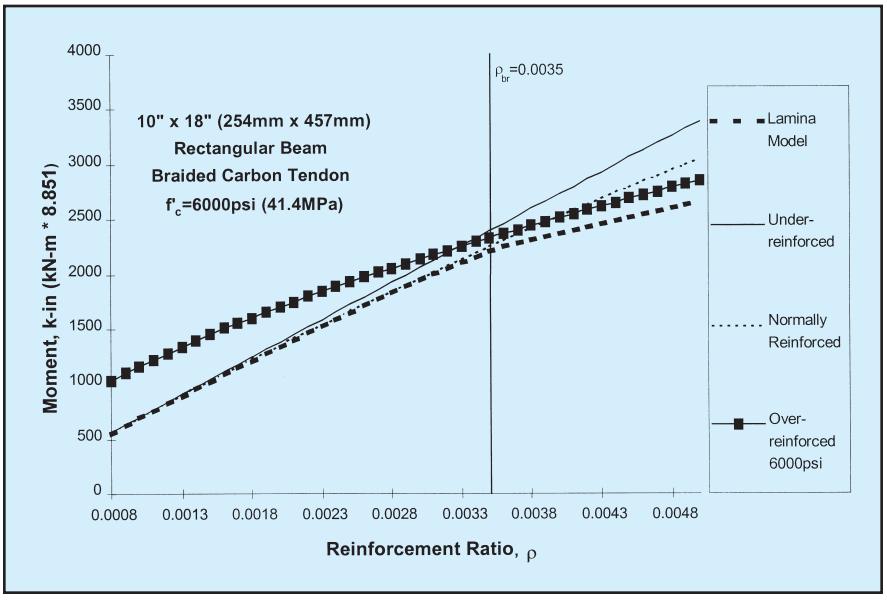

Fig. 2. Typical curve from parametric study of design equations.

Second, the lamina model verified the balanced ratio calculation. The lamina model indicates a transition between the over-reinforced beam curve and the under-reinforced beam curve at the balanced ratio for each beam examined in this study.

Third, high strength concrete did not significantly increase the moment capacity in the over-reinforced region, but high strength concrete was very effective in raising the overall moment capacity when accompanied with increased tendon capacity.

STRENGTH DESIGN ISSUES

The designer must evaluate two issues prior to developing a design:

First, the decision must be made whether the member is over-reinforced or under-reinforced. Second, the maximum initial prestress values must be selected.

Under-Reinforced Versus Over-Reinforced Beam Design

Data for analyzing under-reinforced and over-reinforced beams were taken from Refs. 5, 10 to 16.

Both under- and over-reinforced FRP prestressed beams fail in a brittle mode. Fig. 3 shows the failure of an under-reinforced beam with a reinforcement ratio near the balanced ratio. Currently, a debate exists among researchers regarding which failure mode is most desirable. Some researchers propose that FRP-prestressed beams be designed as over-reinforced members due to an apparent gain in ductility.[9]

The ductility derives from crushing of the concrete and it is marginally greater than the energy absorbed from tendon rupture. Both cases have significantly less ductility than steel prestressed members. Internally prestressed members are typically under-reinforced with the failure being rupture of the tendon.

Most common prestressed shapes are difficult to over-reinforce with internal tendons. Table 2 indicates the number of steel strands needed to exceed the balanced ratio and the maximum number of strands typically placed in the section. Data were taken from the PCI Design Handbook[17] and Rocky Mountain Prestress.[18]

Fig. 3. Bonded FRP prestressed beam after tendon failure $\rho = \rho_{b.}$

Based on this analysis, most FRP prestressed beams will be under-reinforced. If the maximum number of tendons used is governed by allowable stresses instead of beam geometry, if the section is shallow, or if external post-tensioning is used, then the number of tendons can be increased and an over-reinforced condition may occur.

Maximum Initial Prestress

Two factors combine to establish a maximum prestress level in FRP tendons: creep-rupture behavior and reserve strain capacity. Creep-rupture is the failure of an FRP tendon in a finite time interval when the tendon is stressed less than its full tensile strength. FRP tendons are susceptible to creep-rupture at high stress levels. For example, at 90 percent of its tensile capacity, an aramid tendon has a life expectancy of about two hours.[7]

To prevent creep-rupture failure, and to have the design life of the tendon exceed 100 years, the maximum prestress level is limited to 50 to 60 percent of ultimate capacity for carbon tendons and 40 to 50 percent of ultimate capacity for aramid tendons. Glass tendons are not recommended due to their poor creep-rupture characteristics in moist alkaline environments.

The creep-rupture limitation on initial prestress is not as severe as it appears because tendon strain reserve is needed in the tendon for good flexural behavior. Referring to Fig. 1, the flexural strain to failure, ε_{fu}, must be sufficiently large to allow the beam to deform, crack and provide an indication of incipient failure. Limiting the initial

Table 2. Number of steel tendons to over-reinforce typical common prestressed sections.

Section	Number of tendons required to over-reinforce section	Maximum number of steel tendons possible in cross section
8DT12*	48	8
8DT20*	87	12
10DT34*	190	22
4HC6*	12	9
4HC12*	27	8
FS4*	7	6
G-54†	141	28
G-68†	177	28
G-72†	177	28

Sources:
* PCI Design Handbook, Fifth Edition, 1999.[17]
† Rocky Mountain Prestress, Form Data Book.[18]

prestress to 60 percent of ultimate provides the deformability needed to meet these criteria.

Creep-rupture behavior also affects stressing practices. FRP tendons may be overstressed to account for anchor seating losses, but they should not be overstressed for relaxation losses. A portion of relaxation loss comes from the relaxation of the polymer in the tendons. Over-stressing to compensate the polymer relaxation increases the initial strain in the fiber and decreases the creep-rupture life expectancy.

The design approach consists of selection of a section consistent with the nominal moment requirements. The reinforcement ratio is selected using Eq. (5) and an initial estimate for the depth of the compression block. The reinforcement area is computed and a reinforcement pattern is selected. Then, the material strength reduction factor is chosen.

Checking the balanced ratio, selecting the appropriate prediction equation and verifying the nominal moment capacity validates the design. The nominal capacity times the strength reduction factor must exceed the ultimate moment. If not, the process must be repeated.

EXPERIMENTAL CONFIRMATION OF DESIGN APPROACH

To validate this design approach, a series of prestressed concrete beams were designed and constructed using different types of FRP tendons. The tendons included commercial materials and a generic tendon developed for this project. The generic "strawman" tendon is produced by Glasforms Inc., and has a simple cross section that could be produced from any number of fibers and resins. The properties and materials used for this tendon are listed in Table 3.

The T-section design loads were determined to be approximately one-tenth of an AASHTO LRFD Design Tandem. This design truck was chosen for its two-axle layout, which is close to the four-point loading configuration used in flexural testing. Allowable concrete service stresses were defined using the AASHTO LRFD Design Specification (see Table 4).

Table 3. Strawman tendon properties.

	Volume percent	Tensile strength ksi (MPa)	Tensile capacity kips (kN)	Tensile modulus ksi (GPa)	Tensile elongation percent
Shell 9405 Resin/9470 curing agent	35	9.3 (64)	–	401 (1.9)	–
Glasforms carbon fibers	65	650 (4482)	–	34,000 (165)	1.9
Theoretical strawman properties		425 (2935)	34.0 (151.0)	22,240 (108)	1.9
Tested strawman average	–	270 (1862)	21.6 (96.0)	22,240 (146)	1.2
σ	–	8.8 (60.7)	0.70 (3.1)	2 (311)	0.12
Average –1.65 (95% inclusion)		–	20.4 (90.9)	–	–

Table 4. Allowable concrete stresses.

Allowable stresses a transfer of prestress (prior to losses)	
(a) Extreme fiber stress in compression	$0.60 f'_{ci}$
(b) Extreme fiber stress in tension except for Item (c)	$3\sqrt{f'_{ci}}$
(c) Extreme fiber stress in tension at ends	$6\sqrt{f'_{ci}}$
Allowable stresses under service loads (following losses)	
(a) Extreme fiber stress in compression due to prestress plus sustained loads	$0.45 f'_c$
(b) Extreme fiber stress in compression due to prestress plus total loads	$0.60 f'_c$
(c) Extreme fiber stress in precompressed tensile zone	$6\sqrt{f'_c}$

Table 5. Characteristics of test beams.

	Number of tendons	Area of tendons sq in. (mm^2)	P_u kips (kN)	P_i kips (kN)	E_f ksi (GPa)	f'_c psi (MPa)	l ft (mm)
CFCC 1	1	0.12 (76)	26.2 (161)	18.1 (80.5)	20,500 (137)	7400 (49.6)	15.0 (4570)
Fibra 1	1	0.20 (127)	39.6 (176.4)	15.9 (70.6)	10,250 (68.6)	9700 (64.8)	15.0 (4570)
Strawman 1	2	0.078 (50.3)	21.6 (96.2)	12.0 (53.4)	21,800 (146)	6300 (31.0)	15.0 (4877)
Strawman 2	2	– (50.3)	21.6 (96.2)	12.0 (53.4)	21,800 (146)	4600 (31.0)	16.0 (4877)
Strawman 3	1	– (50.3)	21.6 (96.2)	12.0 (53.4)	21,800 (146)	4600 (31.0)	10.0 (3048)

Notes: CFCC = carbon fiber tendon
Fibra 1 = aramid tendon
Strawman = carbon tendon provided from Glasforms Inc.

All of the beams with the exception of Strawman 1 beam were designed with straight tendons. The Strawman 1 beam was designed with two tendons, one straight and one depressed 3 in. (76 mm). The harped tendon was pushed down with a hydraulic jack and a 2 in. (51 mm) long saddle with a radius of curvature of 36 in. (914 mm). The harped tendon was stressed so that the harping action plus the axial prestress would result in the same maximum stress level as the straight tendon.

The stress increase, σ, due to the harping of a solid tendon should be determined by Eq. (10):

$$\sigma = \frac{E_f r}{R} \tag{10}$$

where

E_f = modulus of elasticity of tendon
R = radius of saddle
r = radius of tendon

Five different prestressed beams were designed. Carbon/nylon FRP

stirrups were placed outside the constant moment section at a spacing of *d*/2. No stirrups were placed in the constant moment section of the beam. The details of the test beams are shown in Table 5, their predicted strength is given in Table 6, and the beam cross sections are illustrated in Fig. 4.

Flexural Testing

The beams were loaded with a single 55 kip (245 kN) MTS jack and load cell. A spreader beam created a four-point loading with a 36 in. (914 mm) region of constant moment. Strawman 3 beam had a 12 in. (305 mm) constant moment section due to the shorter length of the beam. The test setup used is shown in Fig. 5.

Data Acquisition

The data acquisition for this project monitored load, deflection, tendon end slip, and crack width. Load readings for the flexural testing were taken directly from the load cell on the MTS jack. Deflections were taken by placing direct current displacement transducers (DCDT) on either side of the beams at midspan. End slip of the tendons was measured by linear potentiometers (LP).

After release of prestress, the excess tendon was removed, leaving a short section protruding from each end of the beam. The LPs were attached to the ends of the tendons and spring-loaded against the end of the beams. The LPs measure end slip of the tendon and provide an indication whether the development of the tendons governed the failure of the beams. Crack width data were taken by loading the beam beyond the cracking load, completely unloading it, and then placing a linear potentiometer across the largest initial crack.

Table 6. Predicted beam behavior and strength.

Beam ID	Tendon type	Condition	Predicted strength kip-ft (kN-m)
CFCC	Carbon	Under-reinforced	27.5 (37.3)
Fibra 1	Aramid	Under-reinforced	18.4 (25.0)
Strawman 1	Carbon	Under-reinforced	30.1 (40.9)
Strawman 2	Carbon	Under-reinforced	30.1 (40.9)
Strawman 3	Carbon	Under-reinforced	13.7 (18.6)

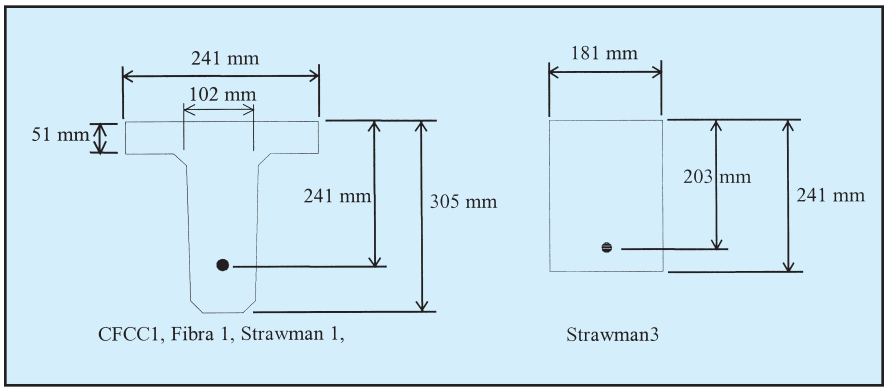

Fig. 4. Cross section of test beams.

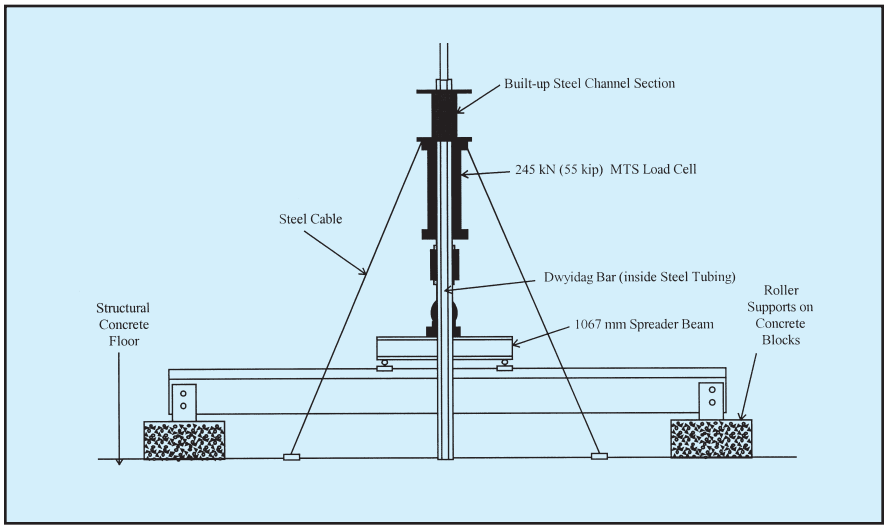

Fig. 5. Testing apparatus setup.

RESULTS OF FLEXURAL STRENGTH CALIBRATION

The design models are compared with the beam behavior to validate the ability to predict the failure mode, the actual strength, and overall tendon behavior and serviceability conditions. Tables 5 and 6 summarize the beam and tendon properties, test setup and test results.

Failure Modes

All of the beams failed by tendon rupture as predicted by the balanced ratio calculation. The failure of the CFCC1 beam was the result of the breakage of a small portion of the tendon outside of the left load point. This resulted in an energy release that caused a long horizontal crack to form at the tendon level and the bottom of the beam breaking off, leaving the remaining tendon exposed.

The beam continued to carry load up to the point where the remaining

Table 7. Predicted and experimental beam results.

	f_{fu} – mean value					f_{fu} – mean value-1.65σ			f_{fu} – mean value-3σ		
Beam	M_{exp} kN-m	M_{calc} kN-m	$\frac{M_{exp}}{M_{calc}}$ ϕ = 1.0	$\frac{M_{exp}}{M_{calc}}$ ϕ = 0.9	$\frac{M_{exp}}{M_{calc}}$ ϕ = 0.85	$\frac{M_{exp}}{M_{calc}}$ ϕ = 1.0	$\frac{M_{exp}}{M_{calc}}$ ϕ = 0.9	$\frac{M_{exp}}{M_{calc}}$ ϕ = 0.85	$\frac{M_{exp}}{M_{calc}}$ ϕ = 1.0	$\frac{M_{exp}}{M_{calc}}$ ϕ = 0.9	$\frac{M_{exp}}{M_{calc}}$ ϕ = 0.85
CFCC1	34.9	37.3	0.936	1.040	1.102	0.996	1.107	1.172	1.051	1.168	1.237
Fibra1*	19.6	25.0	0.783	0.870	0.921	0.816	0.906	0.960	0.845	0.939	0.994
Strawman1	39.2	40.9	0.959	1.066	1.128	1.013	1.126	1.192	1.062	1.180	1.249
Strawman1-2	39.3	40.9	0.960	1.067	1.130	1.014	1.127	1.193	1.063	1.182	1.251
Strawman 3	19.1	18.6	1.027	1.141	1.208	1.084	1.205	1.276	1.137	1.263	1.337

* Only 3σ strength was available; therefore, statistical data were used for a similar aramid tendon to adjust the strengths. The aramid was chosen since it is another braided product and is similar to the Fibra construction.

tendon broke, at a load over 50 percent higher than the load that initiated the initial tendon failure. The initial tendon failure occurred in the center of the beam in a section with no shear reinforcement. The lack of shear reinforcement allowed rapid propagation of the crack in the concrete in the vicinity of the initial tendon "wire" failure.

The Fibra l tendon fractured slightly outside of the left load point. A flexural crack had formed at that location.

The Strawman l tendon fractured simultaneously with a diagonal crack propagating at a low angle through the flange. The failure occurred at a point well outside of the right load point. The longer portion of this beam was retested, resulting in a tendon failure underneath the right load point. There was no apparent tendon damage at the harp point. The Strawman 3 tendon failed outside of the right load point.

Strawman 2 was not tested during this program but was held for long-term durability evaluation. The tendency of the failure point to fall underneath or near one of the load points is due to very slight variations of the load points and tendon eccentricities creating one load point being slightly, more sensitive than the other.

Predicted Versus Experimental Strength

All of the beams failed within 10 percent of the predicted strength, with the exception of the Fibra l beam, which broke at a much lower load than predicted. The lower than predicted strength of the Fibra l beam can be attributed to possible damage to the tendon during stressing or can be attributed to the variation in beams prestressed with aramid tendons as seen in Table 2.

The experimental results are compared to the calculated nominal capacity based on the mean tendon strength, the mean tendon strength reduced by 1.65σ, and the mean tendon strength reduced by 3σ, each with ϕ factors of 1.0, 0.9, and 0.85. These results are summarized in Table 7 and in Figs. 6 , 7, and 8. Figs. 6 through 8 also indicate the increasing conservatism with

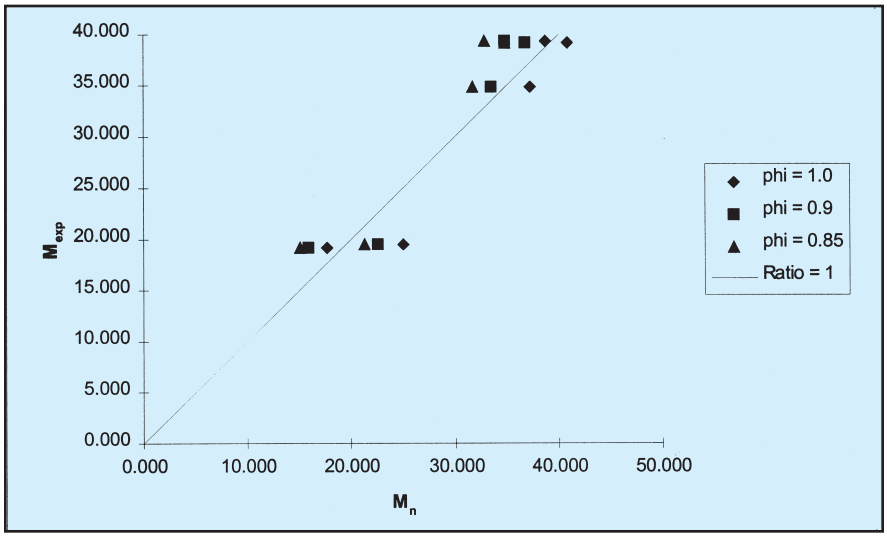

Fig. 6. M_{exp} versus ϕ M_n with mean tendon strength.

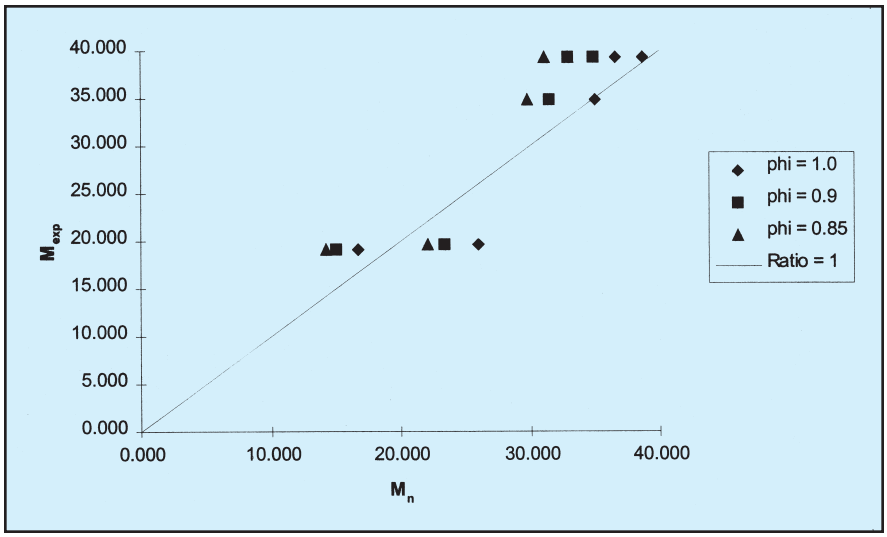

Fig. 7. M_{exp} versus ϕ M_n for mean tendon strength less 1.65σ (95 percent inclusion).

the more restrictive definition of the tendon design strength and lower strength reduction factor. The figures further reflect the Fibra tendon failing at below the expected capacity.

In all the design cases, using the tendon design strength, mean test strength less three standard deviations, and a ϕ factor of 0.85, provided a design prediction greater than the experimental results. A ϕ factor less than 0.85 is desirable for the Fibra tendon. This result is consistent with the results of the larger calibration study presented earlier (see Table 1).

End Slip

No tendon end slip was observed during the testing. The linear potentiometers on the tendons at the ends of the beam showed no movement of any of the tendons. These data imply that adequate bond and development were achieved in all the tendons. Bond development was not a consideration in the nominal moment capacity of any of the beams. The actual embedment length and equivalent strand diameters to the closest failure point are given in Table 8.

This test program was not designed to establish development length but it concludes that full tendon development is attainable within reasonable distances from the beam end. These test results also suggest that the actual tendon design development lengths should be no greater than the values given in Table 8.

Table 8. Minimum bond length to failure point.

Beam	Minimum length from beam end to failure point	
	Length, in. (mm)	Strand diameters
CFCC 1	72.5 (1820)	145
Fibra 1	72.5 (1820)	202
Strawman 1	72.5 (1820)	227
Strawman 3	53.9 (1370)	171

Crack Widths

Monitoring crack width proved inconclusive. The major crack in each beam was instrumented. However, in all three cases, either new cracks formed adjacent to the monitored crack, or a bifurcation occurred and the monitored crack was not representative of the actual crack width. Additional research and testing is ongoing to monitor the crack width behavior.

CONCLUSIONS

The following conclusions for flexural behavior may be drawn from the extended calibration and test validation results:

1. The balanced ratio is effective in defining the transition between the under- and over-reinforced failure modes.

2. The design equations provide an effective method of predicting the flexural strength of bonded FRP prestressed members and may be used for the design for FRP prestressed beams.

3. The tendon design strength, equal to the mean test strength minus three standard deviations, is recommended as the basis of design.

4. The strength reduction factor for flexural design is a function of the tendon type. Based on the calibration analysis, the following ϕ factors are recommended:

$\phi = 0.85$ for carbon tendons

$\phi = 0.70$ for aramid tendons

5. There is more variability in over-reinforced beams than in under-reinforced beams; however, both types of beams are safely predicted.

DESIGN RECOMMENDATIONS

These recommendations address only flexural strength. The following observations will assist the designer in detailing and fabricating FRP prestressed beams.

1. Harping through small angles did not have a significant effect on the Strawman 1 beam. The total angle change for the harped tendon in Strawman 1 was slightly less than 2 degrees. This is only a single test, and more testing needs to be completed to determine if there is a significant reduction in strength with greater harp angles or saddle radii configurations. Safe design procedures should include the increase in stress in the tendon due to curvature in the harping design. This stress increase is given in Eq. (10).

2. The design equations for multiple layers of reinforcement must be calibrated due to the possible rupture of the outermost tendons. These equations and design methodology are provided in Ref. 6.

3. Tendons should be stressed individually to prevent uneven stressing and breakage during the prestressing operation.

4. Use of stirrups over the entire beam length appears to provide sufficient confinement of the concrete in the event of individual fiber breakage in the tendons.

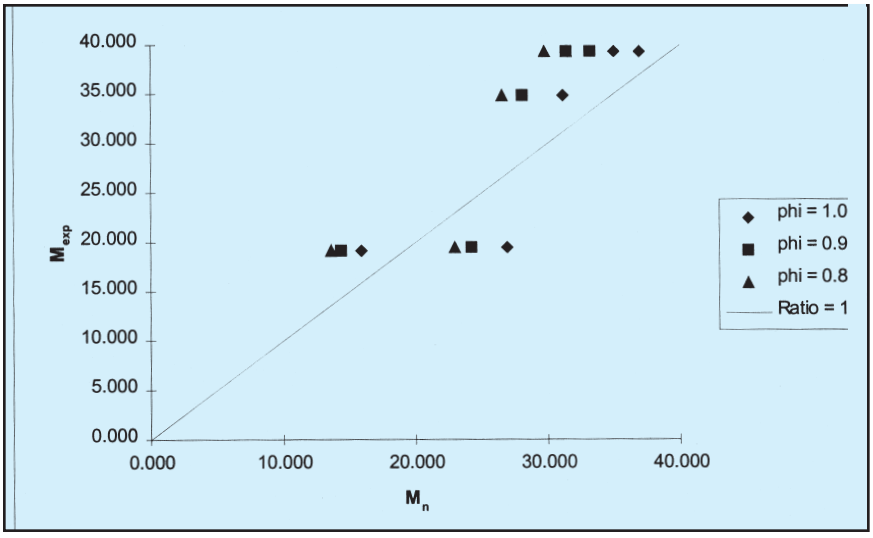

Fig. 8. M_{exp} versus ϕM_n for mean tendon strength less 3σ (design strength).

FUTURE RESEARCH

Completion of a unified design approach requires completion of work on a comprehensive approach to tendon development, serviceability behavior, crack width, creep-rupture, prestress losses, deformability and fatigue behavior. These topics are currently under development by a number of researchers worldwide.

ACKNOWLEDGMENTS

The work presented in this paper is sponsored by the Federal Highway Administration under Contract DTFH61-96-C-0019. The authors wish to thank Eric Munley for his support.

The opinions expressed in this paper are those of the authors and are not construed to represent those of the sponsors.

The authors wish to thank the PCI JOURNAL reviewers of this paper for their insightful and constructive comments.

REFERENCES

1. Gerritse, A., and Werner, J., "ARAPREE – a Non-Metallic Tendon," *Advanced Composite Materials in Civil Engineering Structures*, ASCE, Materials Engineering Division, New York, NY, 1991, pp. 143-154.
2. Dolan, Charles W., "Kevlar Reinforced Prestressing for Bridge Decks," Transportation Research Record 1290, Third Bridge Engineering Conference, Denver, CO, March 1991, pp. 68-75.
3. Gilstrap, J. M., Burke, C. R., Dowden, D. M., and Dolan, C. W., "Development of FRP Reinforcement Guidelines for Prestressed Concrete Structures," *Journal of Composites for Construction*, ASCE, V. 1, No. 4, November 1997, pp. 131-139.
4. Dolan, C. W., and Burke, C. R., "Flexural Strength and Design of FRP Prestressed Beams," Advanced Composite Materials in Bridges – Structures, Second International Symposium, Canadian Society of Civil Engineers, Montreal, Quebec, Canada, 1996, pp. 383-390.
5. Abdelrahman, A., and Rizkalla, S., "Serviceability of Concrete Beams Prestressed by Carbon Fiber-Reinforced-Plastic Bars," *ACI Structural Journal*, V. 94, No. 4, July-August 1997, pp. 447-457.
6. Dolan, C. W., and Swanson, D., "Development of Flexural Capacity of a FRP Prestressed Beam with Vertically Distributed Tendons," Proceedings of ACUN-2, International Composites Conference, University of New South Wales, Sydney, Australia, February 14-18, 2000, pp. 96-101.
7. Leu, B. L., Dolan, C. W., and Hundley, A., "Creep-Rupture of Fiber Reinforced Plastics in a Concrete Environment" FRPRCS-3, V. 2, Sapporo, Japan, October 1997, p. 187.
8. Collins, M. P., and Mitchell, D., *Prestressed Concrete Structures*, Prentice Hall, New York, NY, 1992, p. 61.
9. Grace, N.F., and Sayed, G. A., "Ductility of Bridges Using CFRP Strands," *Concrete International*, V. 20, No. 6, American Concrete Institute, Farmington Hills, MI, June 1998, p. 25.
10. Kakizawa, T., Ohno, S., and Yonezawa, T., "Flexural Behavior and Energy Absorption of Carbon FRP Reinforced Concrete Beams," FRP Reinforcement in Concrete Structures – International Symposium SP-138, American Concrete Institute, Farmington Hills, MI, 1993, pp. 585-598.
11. Taerwe, L., and Matthys, S., "Structural Behavior of Concrete Slabs Prestressed with AFRP Bars," Non-Metallic (FRP) Reinforcement for Concrete Structures, Proceedings of the Second International RILEM Symposium (FRPRCS-2), E - FN SPON, London, United Kingdom, 1995, pp. 421-429.
12. Arockiasamy, M., Zhuang, M., and Sandepudi, K., "Durability Studies on Prestressed Concrete Beams with CFRP Tendons," Non-Metallic (FRP) Reinforcement for Concrete Structures, Proceedings of the Second International RILEM Symposium (FRPRCS-2), E - FN SPON, London, United Kingdom, 1995, pp. 456-462.
13. Zhao, L., "Behavior of Carbon Fiber Composite Tendon Prestressed Concrete Planks Under Static and Fatigue Loading," M.S. Thesis, Department of Civil and Architectural Engineering, Laramie, WY, 1994.
14. Niitani, K., Tezuka, M., and Tamura, T., "Flexural Behavior of Prestressed Concrete Beams Using AFRP Pre-Tensioning Tendons," FRPRCS-3, V. 2, Sapporo, Japan, October 1997, pp. 663-670.
15. Currier, J., "Deformation of Prestressed Concrete Beams with FRP Tendons," M.S. Thesis, Department of Civil and Architectural Engineering, Laramie, WY, 1995.
16. Gowripalan, L., Zou, X. W., and Gilbert, R. I., "Flexural Behavior of Prestressed Beams Using AFRP Tendons and High Strength Concrete," Advanced Composite Materials in Bridges and Structures, 2nd International Conference, Canadian Society for Civil Engineering, Montreal, Quebec, Canada, 1996, pp. 325-333.
17. *PCI Design Handbook – Precast and Prestressed Concrete*, Fifth Edition, Precast/Prestressed Concrete Institute, Chicago, IL, 1999.
18. *Form Design Sections*, Rocky Mountain Prestress, Denver, CO, June 1996.

APPENDIX – NOTATION

a = depth of equivalent rectangular compression block (mm or in.)
A_p = cross-sectional area of prestressed reinforcement in tensile zone (mm^2 or sq in.)
B = number of standard deviations to achieve M_{exp}/M_n = 1.0 (see Table 1)
b = width of compression face of member (mm or in.)
c = distance from extreme compression fiber to neutral axis (mm or in.)
d = distance from centroid of outermost reinforcement to extreme compression fiber (mm or in.)
d_c = distance from centroid of prestressing force to extreme compression fiber for multiple layers of reinforcement (mm or in.)
E_c = modulus of elasticity of concrete (GPa or psi)
E_f = modulus of elasticity of FRP tendon (GPa or psi)
f'_c = specified compressive strength of concrete (MPa or psi)
f'_{ci} = specified concrete compressive strength at time of initial prestress (MPa or psi)
f_{fu} = ultimate tensile stress of FRP strand (MPa or psi)
k = ratio of neutral axis depth to structural depth for beams under service loads
k_u = ratio of neutral axis depth to structural depth for over-reinforced beams
l = length of beam (mm or ft)
M = design moment (kN-m or kip-in.)
M_{exp} = moment capacity established by experimental testing (kN-m or kip-in.)
M_n = nominal moment strength at section (kN-m or kip-in.)
n = modular ratio of elasticity equal to E_f / E_c
P_e = effective prestress force in tendon after losses (kN or kips)
P_i = initial prestress force in tendon (kN or kips)
P_u = ultimate tensile force in tendon (kN or kips)
R = radius of curvature of harping saddle
r = radius of solid tendon
T_u = nominal tensile capacity of FRP tendon (GPa or ksi)
β_1 = factor defined as the ratio of the equivalent rectangular stress block depth to the distance from the extreme compression fiber to the neutral axis depth
ε_{cu} = ultimate compression strain in concrete (0.003)
ε_d = decompression strain, strain in precompressed zone required to bring section back to zero strain
ε_{FRP} = strain in tendon under a specified load
ε_{pi} = initial prestressing strain in prestressed tendon
ε_{fu} = ultimate tensile strain capacity of tendon
ϕ = strength reduction factor
γ = load factor
λ = material constant utilized to calculate k_u
ρ = ratio of prestressed reinforcement equal to A_p/bd
ρ_b = balanced reinforcement ratio
σ = standard deviation for statistical data reduction
σ = stress increase in tendon due to harping